Respiratory Modulation of Sternal Motion in the Context of Seismocardiography

James Skoric, *Member, IEEE*, Yannick D'Mello, Ezz Aboulezz, Siddiqui Hakim, Nathan Clairmonte, Michel A. Lortie, and David V. Plant, *Fellow, IEEE*

***Abstract*—Wearable sensing has enabled physiological monitoring in everyday life. Clinically, cardiovascular and respiratory monitoring commonly requires separate devices. However, for feasibility in wearable systems, they are integrated into a single device. Since seismocardiography (SCG) records the motion of the chest wall, it has the potential to monitor both vital signs. The primary application of SCG is cardiovascular monitoring. As a result, its ability to detect respiration has been less defined. This study characterizes how SCG is affected by respiration and consequently, how respiratory metrics can be derived from these effects. The sternal motion of 40 subjects was recorded using an inertial measurement unit with a spirometer for reference. Three scenarios were examined with the subject at rest, holding their breath at peak inhalation, and holding their breath when exhaled. Three main aspects of respiratory modulation were explored: amplitude modulation, frequency modulation, and baseline wandering. The SCG amplitude was observed to be dependent on respiratory volume whereas baseline and frequency modulation were dependent on inhalation phase. All three effects were employed separately in the calculation of respiratory rate. Estimations from baseline wandering, amplitude modulation, and heart rate modulation produced r-squared values of 0.71, 0.44, and 0.66, respectively. The accuracy of tidal volume measurement was limited by a high inter-subject variability. Estimation of the respiratory waveform produced an average r-squared of 0.76 using multivariate linear regression. This demonstrates the potential of SCG as a tool for respiratory monitoring within an integrated, non-invasive cardiorespiratory monitoring system from a single point of contact.**

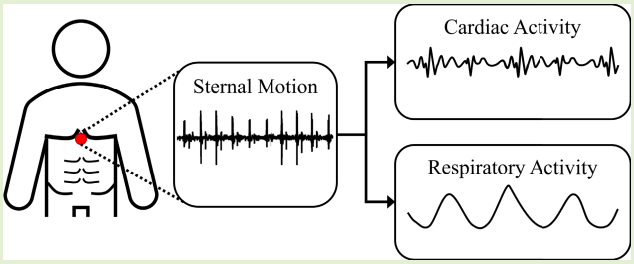

***Index Terms*—Seismocardiography, gyrocardiography, respiration, accelerometers, wearable devices, cardiovascular monitoring.**

I. Introduction

GLOBAL health is threatened by the impact of non-communicable diseases. Their increasing significance has been attributed to unhealthy lifestyles, environment, and an aging population [1]. The most prevalent are cardiovascular and respiratory diseases, which together account for more than 40% of global mortality [2]. The burden of such widespread issues falls on every individual. It implicates national governments and the world economy. This burden is especially severe in low- and middle-income countries [3], [4]. Fortunately, these diseases are preventable by simply avoiding risk factors and maintaining a healthy lifestyle. In the clinic, they are mitigated by monitoring cardiac and respiratory health to detect early symptoms and warning signs [5], [6].

Recently, physiological monitoring has expanded to wearable and non-contact solutions to benefit scenarios outside of the clinic [7]. Sensor-driven approaches promote the value of integrating smart devices into daily life. These portable options are intended to make physiological monitoring more accessible so that people can make informed decisions without needing as many visits to the clinic [8]. This would provide long-term monitoring solutions [9] that expand health coverage to remote locations [10], support low-income individuals [11], and increase health and wellness awareness [12].

The medical standard of non-invasive cardiac monitoring is electrocardiography (ECG), which measures the electrical activity of the heart [13]. Photoplethysmography (PPG) has become a popular and affordable alternative that has been integrated with consumer electronics for fitness and health monitoring. The difficulty with PPG is that it is sensitive to

Manuscript received March 24, 2022; revised May 3, 2022; accepted May 4, 2022. Date of publication May 5, 2022; date of current version July 1, 2022. This work was supported in part by the National Sciences and Engineering Research Council (NSERC) of Canada, in part by MDA Corporation, and in part by McGill University. The associate editor coordinating the review of this article and approving it for publication was Dr. Theerawit Wilaiprasitporn. *(Corresponding author: James Skoric.)*

This work involved human subjects or animals in its research. Approval of all ethical and experimental procedures and protocols was granted by the McGill Research Ethics Board under Application No. 6-0619.

James Skoric, Yannick D'Mello, Ezz Aboulezz, Siddiqui Hakim, Nathan Clairmonte, and David V. Plant are with the Department of Electrical and Computer Engineering, McGill University, Montreal, QC H3A 2T5, Canada (e-mail: james.skoric@mail.mcgill.ca).

Michel A. Lortie is with MDA Corporation, Ottawa, ON K2K 1Y5, Canada.

Digital Object Identifier 10.1109/JSEN.2022.3173205

ambient light and motion artifact [14]. Other technologies such as echocardiography [15], magnetic resonance imaging [16], or high-speed cameras [17], require technical knowledge and are not portable. Seismocardiography (SCG) is a portable and unobstructive method of recording cardiac vibrations on the surface of the chest from a miniaturized accelerometer [18]. It has recently emerged as a strong candidate for cardiac monitoring [19], [20] due to its small form factor and single point of contact with the body [21]. During each heartbeat, vibrations are generated by the movement of the valves and contraction of the heart. Fiducial points in the SCG waveform have been known to accurately correlate with key cardiac time intervals such as the opening and closing of the aortic and mitral valves [22], [23].

In respiratory monitoring, there is no de-facto gold standard with the same ubiquity as ECG for cardiography. Common designs employ either airflow monitoring, chest movement, or indirect techniques. The most accurate method is to use a spirometer to measure air volume. However, this requires the subject to breathe continuously into a tube, which can cause discomfort, and restricts movement during measurement [24], [25]. Therefore, the equipment is not feasible in a wearable monitoring scenario which requires continuous recordings throughout daily life.

A portable, wearable method is respiration inductance plethysmography (RIP), where two bands are wrapped around the torso to monitor expansion. When fitted and calibrated properly, it can provide a highly accurate representation of respiration rate and volume [26]. However, the volumetric measurements are sensitive to changes in posture and position [27] and are infeasible for everyday use.

The fact that both cardiac and respiratory monitoring have been developed separately has led to the need for multiple devices, given that both must be recorded simultaneously. Respiration-specific devices generally have no information regarding cardiac activity. This makes monitoring difficult as cardiac and respiratory functions are inherently coupled, therefore implying that both functions often need to be monitored continuously.

One solution to this issue is to derive respiratory activity from cardiac monitors such as ECG or PPG. ECG-derived respiration (EDR) has been shown to reliably extract respiration rate without the need for a second respiration-specific device [28], [29]. EDR works on the principle that respiration modulates the impedance in the chest and movement of the electrodes, which influences the ECG morphology [30]. Similarly, PPG morphology is modulated by several factors including changes in blood volume and heart rate [29].

SCG also offers a potential solution to integrate both systems into a single device [31]. The benefit of using an inertial measurement unit (IMU) is that it would detect motion related to respiratory activity along with cardio-mechanical activity. Accelerometers can monitor respiration via chest motion using the same principles as RIP [32]. Recent studies have used this motion to monitor respiration with cameras [33], radar [34], ultrasound [35], and wearable strain sensors [36]. Other than using high speed video cameras, most of these methods do not have the granularity needed to record cardiac activity, especially cardiac vibrations. SCG is one of the few tools capable of monitoring both cardiac and respiratory activity at the same time.

The main issue with recording both cardiovascular and respiratory signals from a single sensor is the difficulty of separating the two domains. Since the body is constantly breathing and pumping blood, the two signals are coupled to each other. Respiration modulates the amplitudes and rhythm of cardiac vibrations, similar to the respiratory modulation of ECG and PPG[37]. Several studies have attempted to extract this activity using grouping [38], amplitude change by lung volume [39], breathing estimation from SCG envelopes [40], or machine learning [41]–[44]. However, most studies provide few output parameters [45], employ a limited number of subjects [46], or record respiration from locations unsuitable for SCG [47], [48].

SCG is known as a simple, versatile cardiac monitoring system that can be easily reproduced in a lab environment. However, a better understanding of the respiratory interactions is needed for the technology to become an integrated solution with the same potential as EDR. Therefore, the goal of this study was to statistically analyze the modulation effect that respiration has on a SCG signal. This work characterizes the potential of using SCG as a tool to monitor respiration without any additional hardware. Hence, the sensor system was set up with the intention of recording cardiac vibrations [49]. From this set-up, vibrations were analyzed to determine their modulation due to respiration in terms of amplitude, frequency, and baseline. It expands upon a preliminary version of the baseline modulation which was reported in [50].

From each of these modulation methods, we quantify how they can be interpreted in terms of respiration. The three main evaluation metrics are respiration rate (RR), tidal volume (TV), and respiratory phase (RP). Although RP is not a common respiration metric, it is a useful comparison tool as it verifies how closely the accelerometer signals are aligned with the reference values. The respiratory waveform is then estimated using linear regression. Using these metrics, we evaluate and discuss the effectiveness of using an existing cardiac activity monitoring system for respiratory activity monitoring.

II. Methods

A. Data Acquisition

Data was acquired using a custom-built system which was assembled from commercial, off-the-shelf parts. This enabled a simplified set up that could easily be replicated in other laboratories, demonstrating the accessibility of SCG. Cardiac vibrations were recorded with a single IMU which used an integrated accelerometer and gyroscope (MPU9250, Invensense). The IMU data was polled via an I2C protocol by a Raspberry Pi (Pi-Zero W, Raspberry Pi) at a sampling rate of approximately 600 Hz. The accelerometer and gyroscope were set to a range of ± 2 g and ± 250 deg/sec, respectively. IMU data was saved to a text file on the Raspberry Pi during recording and was then transmitted wirelessly over Wi-Fi to a laptop computer. Additionally, a Biopac digital acquisition system (MP160, Biopac) was used to obtain reference ECG (BN-RSPEC, Biopac) and pneumotachograph (TSD137H, Biopac)

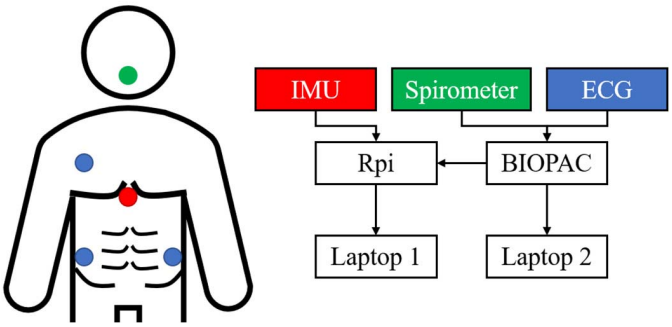

Fig. 1. System schematic showing IMU (Red), ECG (Blue), and spirometer (Green) sensor locations on the body with the corresponding system connections to the Raspberry Pi (Rpi) and BIOPAC systems.

signals. An externally wired clock signal was sent from the Biopac to the Raspberry Pi to create a global timing reference between the two systems. Data was sent serially from the Biopac system to a second computer. *Fig. 1* shows a schematic of the system. Data was combined, synchronized, and analyzed in MATLAB.

The study was conducted on 40 (19 female) healthy participants, with (mean ± standard deviation) age: 24.4 ± 4.6 years, weight: 69.0 ± 13.3 kgs, and height 171.8 ± 10.9 cm. The subjects were tested at McGill University. All subjects had no known prior or existing cardiovascular or respiratory conditions. Study procedures were approved by the McGill Review Ethics Board and consented by the subjects prior to the study. Before testing each subject, the spirometer was calibrated to a 3L reference syringe (AFT27, Biopac). As the de-facto position of SCG recording [19], the IMU was attached to the xiphoid process of the sternum with a piece of double-sided tape. The IMU was placed with the X, Y, and Z axes oriented in the longitudinal, horizontal, and dorsoventral axes of the body, respectively. ECG electrodes were placed on the torso as seen in *Fig. 1*. The study consisted of seven tests as shown in Table I. For the first test, the subject was stationary in a supine position on a massage table. A spirometer with a disposable mouthpiece filter was positioned above the subject's mouth. The subjects were asked to keep a tight seal around the spirometer and breathe normally through only their mouth. No other criteria were set on the rate or depth of their breathing. SCG, spirometer, and ECG were recorded for 3 minutes while the subject was at rest. For the next test, the subject was asked to hold their breath. Our previous work has shown that breath holding was an effective way to isolate the effects of lung volume on the SCG waveform [39]. The spirometer was not used during this test to maximize the subject's comfort and length of breath holding. The subject was asked to inhale fully and hold their breath to a maximum duration of two minutes, or for as long as possible. After a small period of rest, the test was repeated twice. Then, the subject was asked to exhale completely and to hold their breath for as long as possible, or to a maximum of one minute. Again, after some rest, this was repeated twice.

B. Processing

Three forms of modulation were extracted from the signal. Generally, this is represented by equation 1 which shows

TABLE I
SUMMARY OF SUBTESTS

Test	Breathing Type	Length (Minutes)
Rest	Normal Breathing	3
High Lung Volume	Inhaled Breath Hold	2*
High Lung Volume	Inhaled Breath Hold	2*
High Lung Volume	Inhaled Breath Hold	2*
Low Lung Volume	Exhaled Breath Hold	1*
Low Lung Volume	Exhaled Breath Hold	1*
Low Lung Volume	Exhaled Breath Hold	1*

*Indicates maximum length, and most subjects stopped earlier

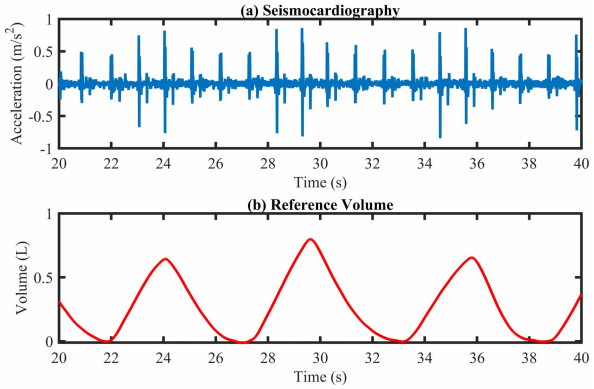

Fig. 2. An example recording during regular breathing of (a) SCG and (b) Respiratory reference volume.

the modulation of a general function of time, $f(t)$, where a represents amplitude modulation, b represents frequency modulation, and c represents baseline wandering (BW).

$$y(t) = a \cdot f(b \cdot t) + c \tag{1}$$

First, timing and amplitudes of two key fiducial points were annotated from the SCG signal. Second, these points were used to obtain the modulation in amplitude and frequency. In the cardiac system, frequency modulation was found to be manifested by modulation in heart rate. Finally, the baseline modulation of the SCG waveform was extracted.

1) Peak Amplitude Modulation: Amplitude modulations challenge autonomous annotation schemes due to the need for variable thresholding on a per breath cycle. One factor of modulation in SCG amplitude was the amount of air in the lungs [39]. When analyzing SCG, it has been demonstrated that grouping beats based on lung volume resulted in higher similarity [38]. This implies that respiratory information can be extracted from the amplitudes of SCG peaks. Other work showed that the upper and lower amplitude envelopes can be used to detect respiratory phases [40]. The amplitude modulation can be seen in *Fig. 2* where SCG amplitude is periodic with the corresponding reference volume over several breath cycles. The largest oscillation amplitudes in the SCG waveform were attributed to the aortic opening (AO) and the isotonic contraction (IC), which can be seen in the single beat shown in *Fig. 3*. These two fiducial markers were analyzed for their relationship with respiration.

ECG was annotated using the Biopac AcqKnowledge software to get R-peak timings. The recordings were segmented

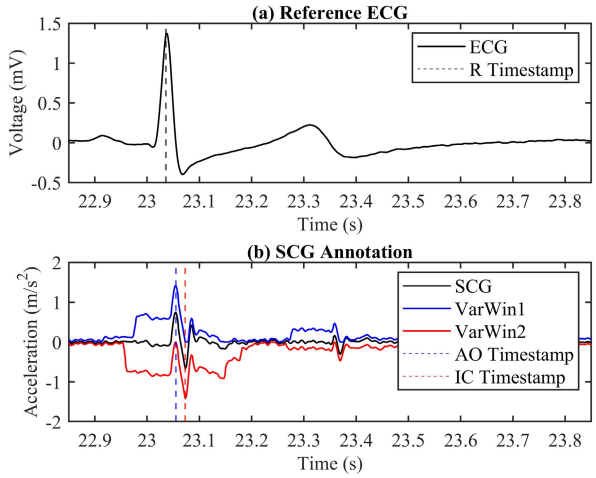

Fig. 3. A single beat shown with (a) reference ECG and highlighted R-Peak, and the (b) SCG annotation process. Filtered SCG is shown in black, VarWin and resulting AO point shown in blue, VarWin and resulting IC point shown in red.

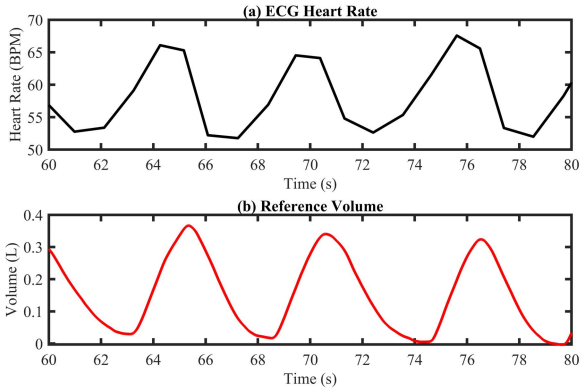

Fig. 4. An example during regular breathing of (a) ECG reference heart rate modulated via (b) Respiration.

into heartbeats with 0.2 seconds prior to the R-peak was used to approximate the start of the cardiac cycle. SCG signals were filtered by a 3rd order Butterworth bandpass filter with cut-off frequencies at 2 and 100 Hz to remove high frequency IMU noise and low frequency baseline oscillations. Features were amplified by a custom-built function which amplifies variations in a window, called VarWin [31]. For each data point, the largest oscillation (difference between local maximum and local minimum) within a window around the point was calculated using this function. Two instances were used to annotate the AO and IC points. A window after the evaluated timestamp was considered in the first instance. This minimized the interference of the rapid ejection (RE) point. The largest swing in amplitude occurred between the AO and IC points, which resulted in a local maximum occurring at the timestamp of the AO point. Only those AO points that occurred within 20 milliseconds following the R-peak were considered. An example of a processed beat is shown in *Fig. 3*. The second VarWin instance employed the same transfer function on negative Z-axis acceleration with a window centered on the evaluated timestamp. The minimum point of this signal occurring within approximately 50 milliseconds following the R-peak was selected as the IC.

2) Heart Rate Modulation: One of the most well-known aspects of cardio-respiratory coupling is the modulation of heart rate by breathing, which also applies to SCG. This is carried out by the autonomous nervous system. With each breath, heart rate is typically increased during inhalation and decreased during exhalation [51]. This is because more oxygen is directed to the respiratory muscles [52] during the active process of inhalation. The same principle occurs during physical activity: the heart rate increases so that more oxygen can be transported to muscles throughout the body [53], with an example shown in *Fig. 4*. The standard method to monitor heart rate is by using ECG R-peak timing [54]. In SCG, the de-facto R-peak surrogate is the AO point; provided there are no electro-mechanical disabilities, the heart rate from AO to AO correlates well with heart rate from R to R [55]. Heart rate was determined from the SCG waveform using the extraction method explained in the previous section. Since both AO and IC points were extracted, both were used to calculate two separate instantaneous heart rates which were directly compared with HR derived from ECG. The fluctuation in SCG-derived HR was used as a measure of frequency modulation and compared to respiratory metrics.

3) Baseline Modulation: During respiration, the lungs fill with air and expand, causing the surface of the chest to rise and fall with each breath. In a common checkup, a doctor or nurse uses this principle to approximate a patient's breathing rate. This motion can be recorded when an IMU is placed on the chest. Structurally, the sternum and upper ribs move upward and outward in a 'pump handle' motion to increase the dorsoventral radius of the chest. As the chest moves outward, the sensor accelerates along the Z-axis. Simultaneously, the lower ribs expand outward and upward in a 'bucket handle' like motion to increase the horizontal radius. As the chest moves upward, the sensor accelerates along the X-axis. An off-center placement of the sensor or nonsymmetric body shape induced additional oscillations in the Y-axis. The gyroscope also experienced oscillation when the surface of the chest rotated, primarily in the X- and Y- axes. This slow periodic movement was found to happen independently from the cardiac beats and was mixed into the IMU signal. This motion was attributed to the baseline wandering of the cardiac beats. Fig. 5 shows an example of the baseline oscillations occurring in the raw IMU signal. In general, some cardiac and respiratory effects can be seen across all three axes. As SCG was primarily recorded from the Z-axis due to its cardiac periodicity, respiration baseline wandering was strongest in the X-axis. Therefore, this work has been centered around extracting baseline wandering from the X-axis.

Through filtration, this signal can be extracted for the analysis of respiratory parameters. The Savitsky-Golay filter [56] is commonly used to remove baseline wandering from physiological signals [57]. A 4th order Savitsky-Golay filter was used to remove both high frequency noise and cardiac vibrations. The window size of the filter was variable depending on the respiratory frequency. To set the window size

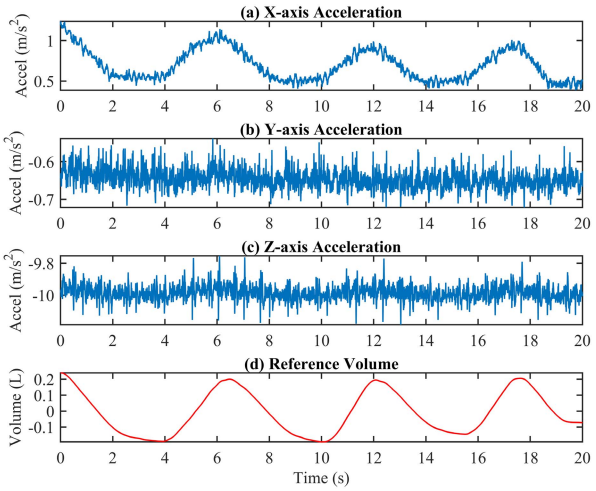

Fig. 5. Raw IMU data during regular breathing for (a) X-axis, (b) Y-axis, (c) Z-axis, and (d) Reference respiratory volume. Periodic baseline oscillations are seen in X-axis acceleration.

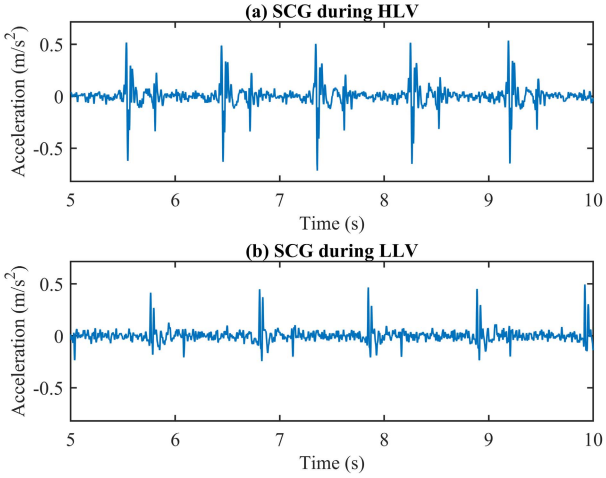

Fig. 6. SCG signal during breath holds for (a) High Lung Volume, and (b) Low Lung Volume for the same subject.

of the filter, the frequency spectra were normalized by their range and summed across all axes. Since respiration was the largest common signal across all the axes, the peak frequency within the 0-2 Hz range was assumed to be the respiratory frequency. The frame length was proportional to this period. The filtered signal was compared to the respiratory waveform and described in section II.C.2.

C. Analysis

After processing the data to extract each of the four main modulation types, these signals were analyzed statistically during breath holds and during normal breathing. The same signals were then used to extract key respiratory parameters during normal breathing.

1) Static Analysis: SCG waveforms have been shown to be modulated by both inhalation phase and volume [58]. While it was not possible to isolate inhalation without a change in volume, it was, in fact, possible to isolate a change in volume without active inhalation. Volume can be isolated from inhalation phase using static breath holds. As the two scenarios were explored, the high lung volume (HLV) and low lung volume (LLV) breath holds allowed for an evaluation of changes in SCG morphology purely due to volume. Neural networks have been capable of classifying these volume states [44]. The morphology effects were shown in [39], where root-mean-squared (RMS) varied due to volume across all 6-axes of an IMU. An example waveform can be seen in Fig. 6 where two signals from the same subject appeared to be different due to a change in lung volume. This past work was applied to the fiducial points of the AO and IC in the new dataset.

The effects were also analyzed to extract baseline and frequency modulation. Baseline modulation was extracted with the window size derived in the subject's initial rest dataset. Each source of modulation was averaged across all three of the HLV and LLV datasets. Both the absolute and relative variation in the signals were analyzed as there was high variation in amplitude, baseline, and HR across subjects. The absolute change was normalized by the average signal value across the entire rest dataset for each subject. The percent change was calculated by the following equation where X represents each accelerometer-derived modulation signal from the previous sections (HR, AO Amplitude, IC Amplitude, or Baseline X).

$$\Delta X = \frac{X_{HLV} - X_{LLV}}{X_{rest}} * 100 \tag{2}$$

where X_{HLV} was the average value from the HLV dataset, X_{LLV} was the average value from the LLV dataset, and X_{rest} was the average value from the rest dataset.

2) Parameter Extraction: After the modulations of the signals was characterized, their mapping to key respiration parameters was determined. In this section, four consistent modulation sources from the previous sections were considered: X-axis baseline, heart rate, AO amplitude, and IC amplitude.

The spirometer flow values were smoothed and integrated to produce respiratory volume. Numerical integration drift was removed by fitting a 2^{nd} order polynomial. The local minima of the reference volume waveform were manually annotated to mark the beginning of each respiration cycle. Only full respiratory cycles were considered in the analysis. To extract tidal volume, the volume from each breath was reset to zero at each annotated local minimum from the respiratory waveform – corresponding to the beginning of the inhalation phase. The following local maximum in each breath corresponded to the tidal volume of that breath. The four accelerometer-derived values were also reset at the minimum value nearest to the start of the volume cycle. The following maximum value per breath was analyzed.

Respiration rate (RR) and respiration phase (RP) could be compared directly to the signals because their units matched. RR was defined as the time difference between successive maximum peaks with a limitation of one peak per respiratory cycle. Respiration phase was defined as the time difference between the reference peak, t_{maxV}, and the signal peak, t_X, and then scaled by the average reference respiratory period,

T_{Resp}, per subject, as shown in the following equation.

$$\phi = \frac{t_{\max V} - t_X}{\text{mean}\left(T_{\text{Resp}}\right)} \times 360 \tag{3}$$

Mapping signal amplitude to TV was more difficult due to a mismatch in units and large inter-subject variability. It was impossible to extract tidal volume from SCG by directly correlating amplitude values because each person a different breathing pattern, movement, and body composition. Therefore, to map the amplitudes to TV and calibrate for personal changes, a linear regression was used for each subject where X was the peak accelerometer-derived modulation value, Y was the tidal volume, n was the number of breaths in the recording, and β were the linear coefficients as seen in the equation below.

$$\begin{bmatrix} 1 & X_1 \\ \vdots & \vdots \\ 1 & X_n \end{bmatrix} \begin{bmatrix} \beta_0 \\ \beta_1 \end{bmatrix} = \begin{bmatrix} Y_1 \\ \vdots \\ Y_n \end{bmatrix} \tag{4}$$

Then a predicted tidal volume, $\hat{Y}$, can be estimated by,

$$\hat{Y} = \beta_1 X + \beta_0. \tag{5}$$

The linear regression allowed for calibration on a per-subject basis while still maintaining the linear relationship between each parameter and tidal volume. All of the data was used for both calibration and prediction.

D. Respiratory Waveform Estimation

The respiratory waveform provided important indications as to the timing, depth, and breathing pattern. The IMU recorded respiratory information from several sources of modulation and therefore could be combined into a single respiratory waveform using sensor fusion [59]. Only the baseline wandering metrics were considered as they were continuous signals unlike the HR and amplitude components that are confined to a per-beat resolution. As respiratory effects were apparent across all 6 axes of motion, they were combined into a single respiratory estimation. Baseline signals were extracted using the procedure outlined in the baseline modulation section. Both IMU and reference volumes were interpolated to a sampling rate of 200 Hz. The reference volume drift was removed with a fitted 2nd order polynomial. The baseline signals were filtered by a 3rd order low pass Butterworth filter with a cutoff of 1 Hz and had their mean value removed. Multiple linear regression was used to fit a linear model between the baseline motion and respiration. A single respiratory waveform signal was predicted using a linear summation of all 6 baseline axes, scaled by linear coefficients and offset. The linear model is shown in equation 6 where $\hat{Y}$ represents the predicted signal, β is each coefficient, a is each acceleration axis, and g is each gyration axis.

$$\hat{Y} = \beta_0 + \beta_1 a_X + \beta_2 a_Y + \beta_3 a_Z + \beta_4 g_X + \beta_5 g_Y + \beta_6 g_Z \tag{6}$$

Past work has shown that due to inter-subject variability, the axis which best aligns to the respiration waveform is subject dependent [50], indicating that regression coefficients should be determined on a per-subject level. Each subject had an optimized model. For each subject, the first sequential 70% of the data was used to train the model with only the last 30% used for validation. The model was also evaluated when a single average coefficient was used across the entire dataset.

TABLE II
DATASET CHARACTERISTICS

Characteristic	Value (±Standard Deviation)
Subjects	40
Cardiac Cycles	23068
Respiration Cycles	1531
Average HR	66 (± 12.2) bpm
Average RR	14.57 (± 6.38) bpm
Average TV	404.80 (± 261.35) mL
Average t_{AO}	14.01 (± 8.45) ms
Average t_{IC}	36.01 (± 12.59) ms

III. RESULTS

The annotation method was verified using heart rate as a comparison in section III.A. Then, static breath holds were used to identify the variation in the signals due to respiration volume in section III.B. The same characterization was performed during normal breathing in section III.C. Using this information, the respiratory parameters (Respiration Rate, Respiration Phase, and Tidal Volume) were extracted in sections III.D, III.E, and III.F, respectively. Finally, the respiratory waveform was estimated using multivariate linear regression in section III.G.

Data was collected from 50 subjects. The data from 10 subjects was discarded due to inconsistencies and artifacts in reference volume, or acquisition errors in at least one of the tests. The remaining 40 subjects were used in the analysis. A summary of the data is shown in Table II. The AO and IC intervals were estimated based on the delay of the timestamps, t_{AO}, and t_{IC}, respectively, from the timestamp of the R-peak. HR and RR are shown in beats per minute (bpm).

A. HR Verification

The first step of the analysis was to verify the annotation of the fiducial points. This ensured that the features were consistent when used for the amplitude and frequency modulation components. It was verified by using heart rate as a comparison metric. The relatively stable time delay between the R-peak, AO, and IC points during successive beats, paired with the variability of HR enabled a direct comparison from each metric to determine proper annotation. Heart rate from AO to AO (HR_{AO}) compared with R to R (HR_R) resulted in a squared correlation coefficient r^2 of 0.999 ($p < 0.001$). Heart rate from IC to IC (HR_{IC}) compared with HR_R resulted in an r^2 of 0.995 ($p < 0.001$). Finally, HR_{IC} compared with HR_{AO} resulted in an r^2 of 0.994 ($p < 0.001$). Given the variation in heart rate between beats, the high correlations between these three heart rate measurements proved that the timing of annotated fiducial points were consistent across the entire dataset. It should be noted that as the R-peak was used to identify the AO, these

TABLE III
RELATIVE AND ABSOLUTE AVERAGE PARAMETER CHANGE BETWEEN STATIC APNEA SUBTESTS

Source	Relative Average Change	Relative Standard Deviation	Absolute Average Change	Absolute Standard Deviation
Baseline X	-24 %	175 %	-0.289 m/s^2	0.416 m/s^2
Heart Rate	-3 %	8 %	-2.2 bpm	5.4 bpm
AO Amplitude	46 %	54 %	0.108 m/s^2	0.122 m/s^2
IC Amplitude	94 %	74 %	0.231 m/s^2	0.191 m/s^2

TABLE IV
RELATIVE AND ABSOLUTE AVERAGE CHANGE PER BREATH

Source	Relative Average Change	Relative Standard Deviation	Absolute Average Change	Absolute Standard Deviation
Baseline X	5 %	111 %	0.23 m/s^2	0.243 m/s^2
Heart Rate	17 %	8 %	10.8 bpm	4.8 bpm
AO Amplitude	51 %	21 %	0.126 m/s^2	0.097 m/s^2
IC Amplitude	61 %	25 %	0.165 m/s^2	0.140 m/s^2

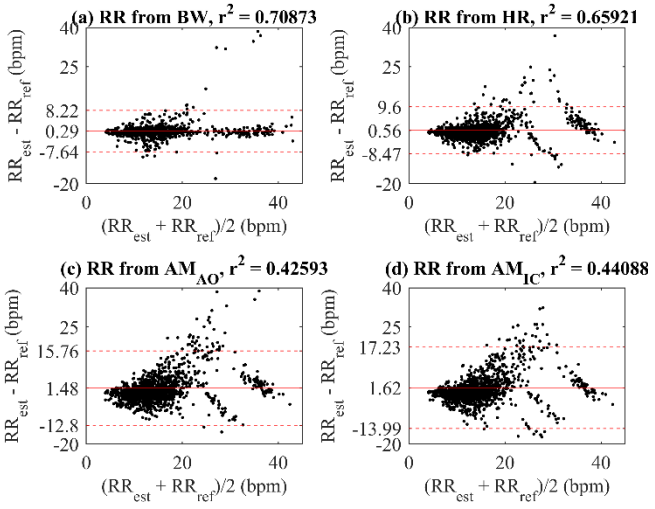

Fig. 7. Bland-Altman plots of estimated (RRest) and reference (RRref) respiration rate with mean (solid red) and 95% limits of agreement (dashed red) for: (a) X-axis baseline wandering, (b) Heart rate, (c) AO amplitude modulation, and (d) IC amplitude modulation.

results did not correspond to the accuracy of a standalone heart rate monitor, which has been described in [31]. The slight imperfections in the correlations can be attributed to the variability of the heart and misclassifications of the points, mainly in the IC point as some recordings produced several indistinguishable local minima.

B. Static Apnea

The SCG signal was analyzed with respect to static breath holds. The relative change from low volume to high volume states was computed due to inter-subject variation. On average, AO amplitudes and IC amplitudes were much larger during HLV than LLV. The IC amplitude produced the largest change with amplitudes 94% greater on average during HLV. Similarly, AO amplitudes were 46% greater on average during HLV. There was no consistent change in baseline X-axis acceleration or heart rate. These findings corresponded with previous work [39] but with finer resolution to the cardiac points and over a larger dataset. As this technique was independent of the effect of inhalation and exhalation, the results demonstrated the dependency of SCG amplitudes on lung volume. Baseline X and heart rate showed no dependency. Additionally, the relative baseline showed a high standard deviation due to the numerical instability of signals oscillating around an acceleration of 0 m/s^2. The average and absolute values across all four metrics are shown in Table III.

C. Normal Breathing

The same analysis from the static apnea subtests was repeated in the resting test. In this scenario, the HLV points corresponded to the maximum value from each source per breath whereas the LLV points corresponded to the minimum value of each source per breath. For example, in one breath, the heartbeat with the highest AO amplitude was the HLV point and the heartbeat with the lowest AO amplitude was the LLV point. A statistical method was therefore used to analyze the largest effects of signal modulation due to respiration. Again, the relative changes were normalized by the average value across the whole set whereas the absolute values showed the change without normalization. Table IV shows the average change and standard deviation within each breath. All four metrics showed an average increase with each respiration cycle. The largest change was IC amplitude, which had a 61% change on average within each respiration cycle. Unlike in the static case, there was a discernable change within each respiratory cycle for both Baseline X and heart rate. Relative Baseline X acceleration again did not provide much information due to the normalization factor but the absolute difference increased by 0.23 m/s^2 on average.

D. Parameter Mapping

1) Respiration Rate: Respiration rate was assessed across all 40 subjects in relation to the four main modulation parameters. RR was extracted as the timing from peak lung volume to peak lung volume in the reference waveform, and from local maximum to local maximum of each of the four parameters. Out of these methods, all produced a noticeable relationship with respiration rate, the most reliable predictor being the baseline X axis, which produced an r^2 of 0.71 ($p < 0.001$). The least reliable predictor was amplitude modulation derived from the AO point, which produced an r^2 of 0.43 ($p < 0.001$). *Fig. 7* shows the correlations between all four methods. As apparent in Figure 7 b)-d), accuracy diminished at high respiration rates. This is common in other beat-to-beat derived methods as well [60]. This was found to be due to the relationship between HR and RR, where a higher RR causes there to be too few heartbeats in each respiratory cycle. Fortunately, as seen in Figure 7a), this limitation was overcome by the baseline wandering method because it was not constrained by the heart rate. The linear correlation, especially at lower RRs, showed that the modulated signals had the same periodicity with the respiration cycle.

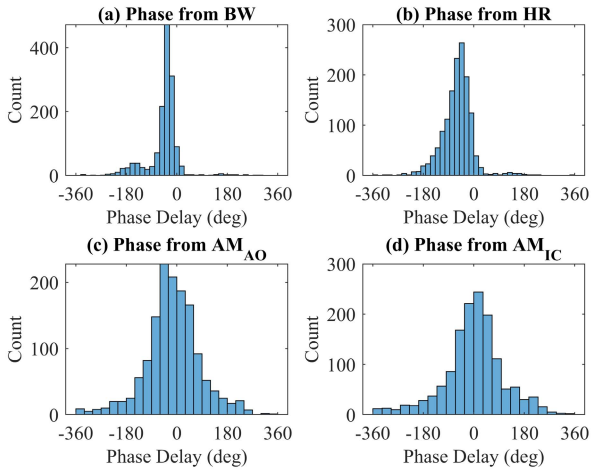

Fig. 8. Histogram of phase delay from (a) X-axis baseline wandering, (b) Heart rate, (c) AO amplitude modulation, and (d) IC amplitude modulation.

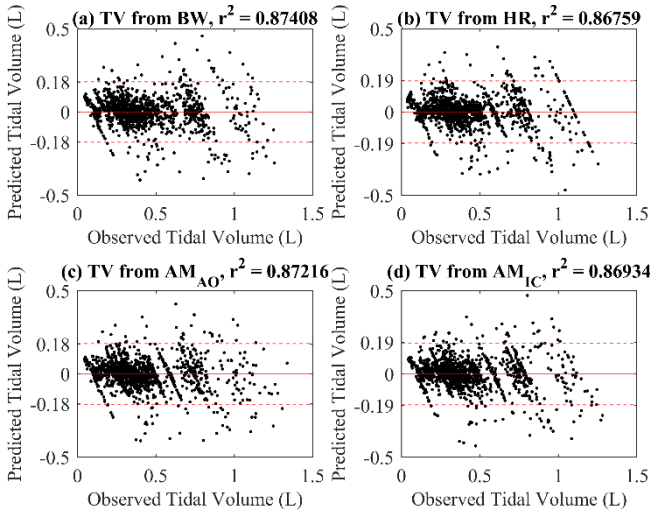

Fig. 9. Bland-Altman plots of estimated (TV_{est}) and reference (TV_{ref}) tidal volume with mean (solid red) and 95% limits of agreement (dashed red) for (a) X-axis baseline wandering, (b) Heart rate, (c) AO amplitude modulation, and (d) IC amplitude modulation.

2) Respiration Phase: The respiration rate results showed that all metrics were periodic with the respiration cycle; however, this did not indicate where in time the cycles aligned. Respiration phase was used to quantify the time delay between the signals. The phase was analyzed using the timing from the peak of each signal to the peak of the reference volume, described in equation 2. *Fig. 8* shows the distribution of the phase delay for each breath across all subjects. The baseline wandering showed a narrow distribution with an average delay of (mean $\pm$ standard deviation) -46 ± 57 degrees. While the distribution had a peak around a delay of -35 degrees, there was a second, smaller peak centered around -180 degrees. This was due to the baseline wandering of some subjects being inverted or perfectly out of phase at -180 degrees. The heart rate modulation resulted in an average delay of -60 ± 56 degrees. Studies have shown that HR modulation corresponds better to inhalation than volume [51], [52], which was verified by the phase timing. The similarity between the HR and baseline wandering showed that it was also dependent on inhalation. Both amplitude modulation sources corresponded to an average delay of 14 ± 98 degrees and 1 ± 107 degrees for the AO and IC amplitudes, respectively. The small delay indicates that signal amplitudes are periodic with respiration volume, as expected from the static case.

3) Tidal Volume: Tidal volume was estimated by mapping the change in each parameter per breath to the volume using linear regression. Across the whole dataset, the results appeared to show a reasonable correlation. *Fig. 9* shows the correlation across the entire dataset where a squared correlation coefficient was around 0.87 for each method. Given that the results of the respiration rate and respiration phase extraction showed variance between methods, it was unlikely that all four signals would converge to approximately the same correlation result. The correlation coefficients for individual subjects were very low where most subjects had a correlation around 0.1 or 0.2. This showed that the global correlation of 0.87 was due to the reference dataset having more variation between subjects than there was within each subject. On average, each subject's reference TV was within a range of ± 400 mL with a standard deviation of 94 mL. In comparison, across the entire dataset, the reference TV occurred over a range of ± 1500 mL with a standard deviation of 262 mL. This indicated that the linear correlation parameters were more dominant in producing linearity than the actual TV estimation due to inter-subject range and deviation. Analysis of variance (ANOVA) was used across all the subjects which indicated that the data from individual subjects were significantly different from the entire dataset ($p < 0.001$). The most reliable signal across all four metrics was the X-axis baseline wandering. The average correlation for the top 10 subjects (25% of the subjects) was 0.56 whereas the bottom 30 subjects (75% of the subjects) was 0.08. This indicated that only some subjects had a linear relationship with TV. This can be seen in *Fig. 9*, where clusters of points were grouped together in a straight line. These points generally occurred from the same subject and indicate that the reference TV was changing whereas the predicted TV did not change. In these cases, the model was not adequate. Therefore, when the dataset was correlated as a whole, the results appeared to be linear, whereas on an individual basis, there was very little correlation.

E. Respiratory Waveform Estimation

Respiration was shown to modulate the recordings in separate ways; however, there was no individual parameter that resulted in the most accurate estimation of the waveform. Additionally, inconsistencies between the subjects required more calibration. Since all or most of the baseline signals showed periodic respiratory modulation, a multiple linear regression was used to combine the sensor readings from each axis. *Fig. 10* shows a comparison between the reference volume and an estimated volume using an individually optimized regression.

This process was completed across all 40 subjects. Squared correlation coefficients were calculated for each subject

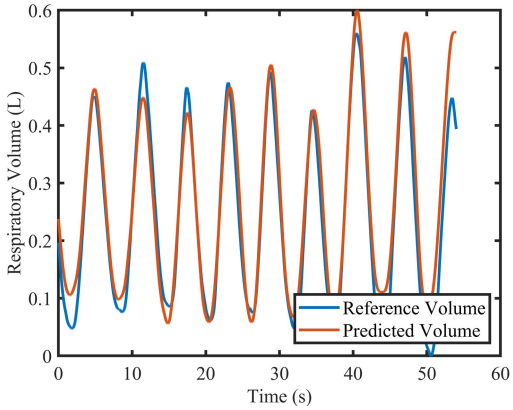

Fig. 10. Respiratory waveform prediction (red) and reference volume (blue) from a single subject.

individually. The average r^2 across all subjects was 0.764. The average predicted equation is shown below where $\hat{Y}$ represents the predicted signal, a is each acceleration axis, and g is each gyration axis.

$$\hat{Y} = 50.17 + 0.538a_X + 0.148a_Y + 4.95a_Z + 0.02g_X - 0.094g_Y - 0.046g_Z \quad (7)$$

As each of the axes was not equal in the magnitude of their variation, the coefficients alone were not a direct indicator of feature importance. Each of the predicted coefficients was scaled by the standard deviation of the corresponding axis to determine the importance of the feature. By this method, the axes were ordered by significance in predicting respiration as: a_x, a_z, a_y, g_y, g_x, g_z.

A new model was generated for each subject. For some applications or for expanding to new subjects, this was not always feasible. A single model derived from the average coefficients of equation 5 was tested for generalizability. This single model resulted in an average r^2 of 0.480. This represented prediction without any per-subject personalization. For comparison, a regression on just the X-axis acceleration alone had an average r^2 of 0.430. This showed that subject-specific parameters were important for predicting the respiratory waveform and that without it the results were not much better than using just the X-axis for estimation.

F. Comparison With ECG-Derived Respiration

The R-wave angle (Rθ) method was used to extract the respiratory signal from the ECG signal because it provided the best results in literature [30] and in our experiments. It was defined [61] as the angle between the upper and lower slopes of the QRS complex. Using the same dataset, Rθ was processed with the same parameter mapping process built for the SCG modulations. For respiration rate, Rθ produced an r^2 of 0.61. This was lower than the r^2 from BW (0.71) and HR (0.66), but higher than AO (0.43) and IC (0.44). As Rθ was extracted on a per-beat basis, the accuracy was similarly degraded at higher RR rates. For respiration phase, Rθ had an average delay of -50 ± 78 degrees, which showed similarity to the BW (-46 ± 57 degrees) and HR (-60 ± 56 degrees). For tidal volume, Rθ had similar results to SCG with a high correlation overall due to the variance in the dataset, but an average per-subject correlation of just 0.15.

IV. Discussion

The annotation schemes provided consistent and reliable detection of the fiducial points on the SCG waveform. By using the HR verification method, it was shown that either could be used as a substitute for the RR interval. The study was limited to the AO and IC points because they were consistently recognizable across all subjects. Several points could be included which might have high impact, particularly the rapid ejection (RE) which follows IC. A second option would be to consider the points near the second heart sound, namely the aortic closing (AC) and mitral opening (MO) points. Their amplitude and interval durations could be analyzed with respect to respiration. These fiducial points had too much variability in the dataset to be consistently defined and were therefore excluded. Additionally, a final application should use an annotation scheme that does not rely on the ECG, as it creates the need for additional hardware.

The static scenarios showed a large change in AO and IC amplitude but less of a change in Baseline X or HR. This showed that HR was susceptible to the act of inhalation but not to the volume itself. HR was shown to be slightly higher for the LLV scenario, although this could be attributed to the test being more difficult and stressful [62].

Using metrics that depended on discrete heartbeats limited the resolution per breath. Amplitude modulation techniques showed a much greater range over static and dynamic tests, although they lacked resolution in the exact phase estimation and therefore had a high standard deviation. This was amplified in scenarios with a relatively high RR.

There was a large range of accuracy deviation between subjects. Some subjects showed little or no correlation to any of the parameters compared to others that showed almost perfect correlation. Several subjects even showed better correlations when using an inverted signal [50]. Although this work did not determine the causation, it could be attributed to sensor placement, body shape, or breathing patterns. It is important to note that many similar studies use only a few subjects [46], which might not be applicable to a broad set of subjects.

Tidal volume estimation was limited in this study. It was shown that in a 3-minute recording, there was not enough variation in breathing depth to produce accurate correlation. Conversely, there was too much variation between subjects in tidal volume to be able to characterize the set as a whole. This was identified as a limitation of the study and should be expanded to longer recordings with variations in subject breath depths. Variation in breath depths, rates, and patterns would also benefit all aspects of this paper. This could be incorporated in future studies to characterize the accuracy and functional range of using SCG as a respiration monitor. The study also focused on linear relationships between the signals and respiration parameters. It is possible that tidal volume can only be estimated using a more detailed relationship or advanced processing.

The results showed that the most reliable method across all respiration metrics (rate, volume, and phase) was the baseline wandering approach. The analysis was constrained to the X axis because it had the strongest periodic oscillations. However, all 3 axes of acceleration and 3 axes of gyration showed some form of oscillation, albeit less consistently than that of the X axis. Therefore, a multiple linear regression was used to fuse all 6 axes together and create a single estimated respiratory waveform. An equation was made for each subject; however, an extension would be to build an algorithm that employs the physical relationships between signals to fuse these metrics into a reliable derivation of respiratory motion.

Additionally, all aspects explored in this work could be extended to better incorporate the gyroscope recordings into the methods. For example, amplitude modulation was not implemented on the gyroscope axes due to a limited knowledge and definition of fiducial points. The gyroscope features previously showed that the gyro Y-axis exhibited the greatest lung volume modulation [39]. Most of the features used in this work provided at least some relationship with respiration; however, the best-case parameter varied on a per-subject basis. An extension would be to build an algorithm that fuses these metrics to reliably predict respiratory parameters, similar to the linear regression model.

This study was conducted in a controlled environment where there were no aspects of noise or motion artifact. In the real world, motion artifact is one of the largest sources of error. Therefore, a real-time estimation algorithm must include some type of filtering, cancelation, or tracking to handle motion artifacts and signal corruption. There have been several studies that provide SCG-specific algorithms; however, these mainly focus on estimating HR [63], [64] and their applicability towards estimating respiratory information was not explored. In this study, corrupted signals were disregarded, although they may still contain useful information if corrected by an algorithm. Additionally, because the subjects recruited in this study were young and healthy, the effects might not be represented in a more general population. The next phase of this work will characterize the methods over more challenging situations such as exercise, deep breathing, and daily activities. This will improve practical utility of our approach and its application as a wearable monitoring solution.

V. Conclusion

The objective of this work was to analyze SCG waveforms in the context of characterizing the modulation due to respiration. 40 subjects were considered for analysis. Four main sources of modulation were described: AO amplitude, IC amplitude, Baseline-X, and heart rate. The findings from the static scenario showed that AO and IC amplitudes were 46% and 94% greater due to lung volume when isolated from inhalation. All four signals showed considerable modulated effects during normal breathing, with IC amplitudes corresponding to the greatest modulation by 64% on average. Respiration rate could reasonably be extracted from all four signals directly, with the most reliable method being Baseline-X with an r-squared of 0.71. Baseline-X and heart rate corresponded to modulation by inhalation due to the lack of static apnea modulation and phase delay from peak respiratory volume. Conversely, the phase of the amplitude modulation aligned to respiratory volume, which was consistent with the static apnea results. Tidal volume could not be extracted directly from any individual parameter. A multiple linear regression was used to estimate the respiratory waveform from the baseline wandering of all six axes with an average r-squared of 0.764. This study outlined the effects of respiration on all aspects of the SCG waveform. These effects could be incorporated into cardiac algorithms to improve detection and be leveraged to provide information on respiratory activity. This will grow the advantage of SCG as a single point of contact sensor to integrate with respiratory and cardiac monitoring.

References

[1] R. Nugent *et al.*, "Investing in non-communicable disease prevention and management to advance the sustainable development goals," *Lancet*, vol. 391, no. 10134, pp. 2029–2035, May 2018.

[2] R. Lozano *et al.*, "Global and regional mortality from 235 causes of death for 20 age groups in 1990 and 2010: A systematic analysis for the global burden of disease study 2010," *Lancet*, vol. 380, no. 9859, pp. 2095–2128, 2012.

[3] B. J. Gersh *et al.*, "Novel therapeutic concepts the epidemic of cardiovascular disease in the developing world: Global implications," *Eur. Heart J.*, vol. 31, no. 6, pp. 642–648, 2010.

[4] P. Burney, D. Jarvis, and R. Perez-Padilla, "The global burden of chronic respiratory disease in adults," *Int. J. Tuberculosis Lung Disease*, vol. 19, no. 1, pp. 10–20, Jan. 2015.

[5] D. Yach, C. Hawkes, C. L. Gould, and K. J. Hofman, "The global burden of chronic diseases: Overcoming impediments to prevention and control," *Jama*, vol. 291, no. 21, pp. 2616–2622, 2004.

[6] A. L. Bui and G. C. Fonarow, "Home monitoring for heart failure management," *J. Amer. College Cardiol.*, vol. 59, no. 2, pp. 97–104, 2012.

[7] I. C. Jeong, D. Bychkov, and P. C. Searson, "Wearable devices for precision medicine and health state monitoring," *IEEE Trans. Biomed. Eng.*, vol. 66, no. 5, pp. 1242–1258, May 2019.

[8] J. Dunn, R. Runge, and M. Snyder, "Wearables and the medical revolution," *Personalized Med.*, vol. 15, no. 5, pp. 429–448, Sep. 2018.

[9] E. Nemati, M. J. Deen, and T. Mondal, "A wireless wearable ECG sensor for long-term applications," *IEEE Commun. Mag.*, vol. 50, no. 1, pp. 36–43, Jan. 2012.

[10] R. Steele and A. Lo, "Telehealth and ubiquitous computing for bandwidth-constrained rural and remote areas," *Pers. Ubiquitous Comput.*, vol. 17, no. 3, pp. 533–543, Mar. 2013.

[11] H. Saksono, C. Castaneda-Sceppa, J. Hoffman, M. S. El-Nasr, V. Morris, and A. G. Parker, "Family health promotion in low-SES neighborhoods: A two-month study of wearable activity tracking," in *Proc. CHI Conf. Hum. Factors Comput. Syst.*, 2018, pp. 1–13.

[12] L. Piwek, D. A. Ellis, S. Andrews, and A. Joinson, "The rise of consumer health wearables: Promises and barriers," *PLOS Med.*, vol. 13, no. 2, Feb. 2016, Art. no. e1001953.

[13] G. S. Wagner, *Marriott's Practical Electrocardiography*. Philadelphia, PA, USA: Lippincott Williams & Wilkins, 2001.

[14] B. S. Kim and S. K. Yoo, "Motion artifact reduction in photoplethysmography using independent component analysis," *IEEE Trans. Biomed. Eng.*, vol. 53, no. 3, pp. 566–568, Mar. 2006.

[15] J. Gottdiener *et al.*, "American society of echocardiography recommendations for use of echocardiography in clinical trials: A report from the American society of echocardiography's guidelines and standards committee and the task force on echocardiography in clinical trials," *J. Amer. Soc. Echocardiogr.*, vol. 17, no. 10, pp. 1086–1119, Oct. 2004.

[16] J. Bogaert, S. Dymarkowski, A. M. Taylor, and V. Muthurangu, *Clinical Cardiac MRI*. Berlin, Germany: Springer, 2012.

[17] I. C. Jeong and J. Finkelstein, "Introducing contactless assessment of heart rate variability using high speed video camera," in *Proc. 36th IEEE Sarnoff Symp.*, Sep. 2015, pp. 7–11.

[18] J. M. Zanetti and D. M. Salerno, "Seismocardiography: A technique for recording precordial acceleration," in *Proc. Comput.-Based Med. Syst. 4th Annu. IEEE Symp.*, Jan. 1991, pp. 4–5.

[19] A. Taebi, B. E. Solar, A. J. Bomar, R. H. Sandler, and H. A. Mansy, "Recent advances in seismocardiography," *Vibration*, vol. 2, no. 1, pp. 64–86, 2019.

[20] O. T. Inan *et al.*, "Ballistocardiography and seismocardiography: A review of recent advances," *IEEE J. Biomed. Health Informat.*, vol. 19, no. 4, pp. 1414–1427, Jul. 2015.

[21] M. D. Rienzo *et al.*, "Wearable seismocardiography: Towards a beat-by-beat assessment of cardiac mechanics in ambulant subjects," *Autonomic Neurosci.*, vol. 178, nos. 1–2, pp. 50–59, 2013.

[22] D. M. Quarrie and P. Neary, "Comparison of seismocardiography to echocardiography for measuring cardiac cycle events," presented at the 6th Annu. Univ. Regina Graduate Student Res. Conf., Regina, SK, Canada, 2011.

[23] R. Crow, P. Hannan, D. Jacobs, L. Hedquist, and D. M. Salerno, "Relationship between seismocardiogram and echocardiogram for events in the cardiac cycle," *Amer. J. Noninvasive Cardiol.*, vol. 8, no. 1, pp. 39–46, 1994.

[24] A. F. T. Hobbes, "A comparison of methods of calibrating the pneumotachograph," *Brit. J. Anaesthesia*, vol. 39, no. 11, pp. 899–907, Nov. 1967.

[25] M. R. Miller, S. A. Dickinson, and D. J. Hitchings, "The accuracy of portable peak flow meters," *Thorax*, vol. 47, no. 11, pp. 904–909, Nov. 1992.

[26] G. K. Wolf and J. H. Arnold, "Noninvasive assessment of lung volume: Respiratory inductance plethysmography and electrical impedance tomography," *Crit. Care Med.*, vol. 33, pp. S163–S169, Mar. 2005.

[27] J. Stradling, G. Chadwick, C. Quirk, and T. Phillips, "Respiratory inductance plethysmography: Calibration techniques, their validation and the effects of posture," *Bull. Europeen Physiopathologie Respiratoire*, vol. 21, no. 4, pp. 317–324, 1985.

[28] G. B. Moody, R. G. Mark, A. Zoccola, and S. Mantero, "Derivation of respiratory signals from multi-lead ECGs," *Comput. Cardiol.*, vol. 12, pp. 113–116, Sep. 1985.

[29] P. H. Charlton, T. Bonnici, L. Tarassenko, D. A. Clifton, R. Beale, and P. J. Watkinson, "An assessment of algorithms to estimate respiratory rate from the electrocardiogram and photoplethysmogram," *Physiol. Meas.*, vol. 37, no. 4, p. 610, 2016.

[30] C. Varon *et al.*, "A comparative study of ECG-derived respiration in ambulatory monitoring using the single-lead ECG," *Sci. Rep.*, vol. 10, no. 1, pp. 1–14, Dec. 2020.

[31] Y. D'Mello *et al.*, "Autocorrelated differential algorithm for real-time seismocardiography analysis," *IEEE Sensors J.*, vol. 19, no. 13, pp. 5127–5140, Jul. 2019.

[32] A. Bricout, J. Fontecave-Jallon, D. Colas, G. Gerard, J.-L. Pepin, and P.-Y. Gumery, "Adaptive accelerometry derived respiration: Comparison with respiratory inductance plethysmography during sleep," in *Proc. 41st Annu. Int. Conf. IEEE Eng. Med. Biol. Soc. (EMBC)*, Jul. 2019, pp. 6714–6717.

[33] S. Transue, P. Nguyen, T. Vu, and M.-H. Choi, "Real-time tidal volume estimation using iso-surface reconstruction," in *Proc. IEEE 1st Int. Conf. Connected Health, Appl., Syst. Eng. Technol. (CHASE)*, Jun. 2016, pp. 209–218.

[34] Y. S. Lee, P. N. Pathirana, C. L. Steinfort, and T. Caelli, "Monitoring and analysis of respiratory patterns using microwave Doppler radar," *IEEE J. Transl. Eng. Health Med.*, vol. 2, pp. 1–12, 2014, Art. no. 1800912.

[35] A. Shahshahani, C. Laverdiere, S. Bhadra, and Z. Zilic, "Ultrasound sensors for diaphragm motion tracking: An application in non-invasive respiratory monitoring," *Sensors*, vol. 18, no. 8, p. 2617, Aug. 2018.

[36] M. Chu *et al.*, "Respiration rate and volume measurements using wearable strain sensors," *npj Digit. Med.*, vol. 2, no. 1, pp. 1–9, Dec. 2019.

[37] P. H. Charlton *et al.*, "Breathing rate estimation from the electrocardiogram and photoplethysmogram: A review," *IEEE Rev. Biomed. Eng.*, vol. 11, pp. 2–20, 2018.

[38] A. Taebi and H. A. Mansy, "Grouping similar seismocardiographic signals using respiratory information," in *Proc. IEEE Signal Process. Med. Biol. Symp. (SPMB)*, Dec. 2017, pp. 1–6.

[39] J. Skoric, Y. D'Mello, M. Lortie, S. Gagnon, and D. V. Plant, "Effect of static respiratory volume on the waveform of cardiac-induced sternal vibrations," in *Proc. 41st Annu. Int. Conf. IEEE Eng. Med. Biol. Soc. (EMBC)*, Jul. 2019, pp. 4917–4921.

[40] N. Alamdari, K. Tavakolian, V. Zakeri, R. Fazel-Rezai, and A. Akhbardeh, "A morphological approach to detect respiratory phases of seismocardiogram," in *Proc. 38th Annu. Int. Conf. IEEE Eng. Med. Biol. Soc. (EMBC)*, Aug. 2016, pp. 4272–4275.

[41] V. Zakeri, A. Akhbardeh, N. Alamdari, R. Fazel-Rezai, M. Paukkunen, and K. Tavakolian, "Analyzing seismocardiogram cycles to identify the respiratory phases," *IEEE Trans. Biomed. Eng.*, vol. 64, no. 8, pp. 1786–1792, Aug. 2017.

[42] P. T. Gamage, M. K. Azad, A. Taebi, R. H. Sandler, and H. A. Mansy, "Clustering seismocardiographic events using unsupervised machine learning," in *Proc. IEEE Signal Process. Med. Biol. Symp. (SPMB)*, Dec. 2018, pp. 1–5.

[43] C. Ulrich *et al.*, "Determining the respiratory state from a seismocardiographic signal—A machine learning approach," in *Proc. Comput. Cardiol. Conf. (CinC)*, Dec. 2018, pp. 1–4.

[44] N. Clairmonte *et al.*, "Neural network-based classification of static lung volume states using vibrational cardiography," in *Proc. 42nd Annu. Int. Conf. IEEE Eng. Med. Biol. Soc. (EMBC)*, Jul. 2020, pp. 221–224.

[45] J.-W. Yoon, Y.-S. Noh, Y.-S. Kwon, W.-K. Kim, and H.-R. Yoon, "Improvement of dynamic respiration monitoring through sensor fusion of accelerometer and gyro-sensor," *J. Electr. Eng. Technol.*, vol. 9, no. 1, pp. 334–343, 2014.

[46] G. Karacocuk *et al.*, "Inertial sensor-based respiration analysis," *IEEE Trans. Instrum. Meas.*, vol. 68, no. 11, pp. 4268–4275, Nov. 2019.

[47] A. R. Fekr, K. Radecka, and Z. Zilic, "Design and evaluation of an intelligent remote tidal volume variability monitoring system in e-health applications," *IEEE J. Biomed. Health Informat.*, vol. 19, no. 5, pp. 1532–1548, Sep. 2015.

[48] A. Jin, B. Yin, G. Morren, H. Duric, and R. M. Aarts, "Performance evaluation of a tri-axial accelerometry-based respiration monitoring for ambient assisted living," in *Proc. Annu. Int. Conf. IEEE Eng. Med. Biol. Soc.*, Sep. 2009, pp. 5677–5680.

[49] Y. D'Mello *et al.*, "Real-time cardiac beat detection and heart rate monitoring from combined seismocardiography and gyrocardiography," *Sensors*, vol. 19, no. 16, p. 3472, Aug. 2019.

[50] J. Skoric *et al.*, "Relationship of the respiration waveform to a chest Worn inertial sensor," in *Proc. 42nd Annu. Int. Conf. IEEE Eng. Med. Biol. Soc. (EMBC)*, Jul. 2020, pp. 2732–2735.

[51] G. G. Berntson, J. T. Cacioppo, and K. S. Quigley, "Respiratory sinus arrhythmia: Autonomic origins, physiological mechanisms, and psychophysiological implications," *Psychophysiology*, vol. 30, no. 2, pp. 183–196, 1993.

[52] F. Yasuma and J. Hayano, "Respiratory sinus arrhythmia: Why does the heartbeat synchronize with respiratory rhythm?" *Chest*, vol. 125, no. 2, pp. 683–690, 2004.

[53] R. Klabunde, *Cardiovascular Physiology Concepts*. Philadelphia, PA, USA: Lippincott Williams & Wilkins, 2011.

[54] J. Achten and A. E. Jeukendrup, "Heart rate monitoring," *Sports Med.*, vol. 33, no. 7, pp. 517–538, 2003.

[55] A. Laurin, A. Blaber, and K. Tavakolian, "Seismocardiograms return valid heart rate variability indices," in *Proc. Comput. Cardiol.*, Sep. 2013, pp. 413–416.

[56] R. Schafer, "What is a Savitzky-Golay filter?" *IEEE Signal Process. Mag.*, vol. 28, no. 4, pp. 111–117, Jul. 2011.

[57] K. T. Nahiyan and A. A. Amin, "Removal of ECG baseline wander using Savitzky-Golay filter based method," *Bangladesh J. Med. Phys.*, vol. 8, no. 1, pp. 32–45, Sep. 2017.

[58] K. Pandia, O. T. Inan, G. T. Kovacs, and L. Giovangrandi, "Extracting respiratory information from seismocardiogram signals acquired on the chest using a miniature accelerometer," *Physiolog. Meas.*, vol. 33, no. 10, p. 1643, 2012.

[59] C. Orphanidou, "Derivation of respiration rate from ambulatory ECG and PPG using ensemble empirical mode decomposition: Comparison and fusion," *Comput. Biol. Med.*, vol. 81, pp. 45–54, Feb. 2017.

[60] J. Lazaro *et al.*, "Electrocardiogram derived respiratory rate using a wearable armband," *IEEE Trans. Biomed. Eng.*, vol. 68, no. 3, pp. 1056–1065, Mar. 2021.

[61] J. Lázaro *et al.*, "Electrocardiogram derived respiratory rate from QRS slopes and R-wave angle," *Ann. Biomed. Eng.*, vol. 42, no. 10, pp. 2072–2083, Oct. 2014.

[62] G. G. Berntson and J. T. Cacioppo, "Heart rate variability: Stress and psychiatric conditions," *Dyn. Electrocardiogr.*, vol. 41, no. 2, pp. 57–64, 2004.

[63] C. Yang and N. Tavassolian, "An independent component analysis approach to motion noise cancelation of cardio-mechanical signals," *IEEE Trans. Biomed. Eng.*, vol. 66, no. 3, pp. 784–793, Mar. 2019.

[64] S. Yu, Q. Song, and S. Liu, "Motion artifact cancellation from a single channel SCG using adaptive forgetting factor recursive least square filter," *IEEE Access*, early access, Sep. 31, 2020, doi: 10.1109/ACCESS.2020.3013380.

James Skoric (Member, IEEE) received the B.Eng. and M.Sc. degrees in electrical engineering from McGill University, Montreal, QC, Canada, in 2018 and 2020, respectively, where he is currently pursuing the Ph.D. degree in electrical engineering. His research is focused on developing seismocardiography sensors for real world applications. His research interests include wearable sensors, physiological monitoring, biomedical signal processing, and remote health monitoring.

Yannick D'Mello received the B.Eng. degree in physics with a minor in economics from Carleton University, Ottawa, ON, Canada, in 2015. He is pursuing the Ph.D. degree with McGill University. He is also the CEO of Stocate. He is passionate about employing technology to benefit society and the natural world. His research interests include sustainability, systems-level optimization processes, energy-matter interactions, wave propagation, signal processing, materials engineering, and autonomous health monitoring.

Ezz Aboulezz received the B.Eng. degree in electrical engineering from McGill University, Montreal, QC, Canada, in 2020. His focus was in programming, electronics, and telecommunications. He is currently a Co-Founder, a CTO, and a Treasurer of the Board at Stocate. He handles business development and technological strategy. He is also a full-time Software Developer at SuccessFinder. Through his journey with Stocate, he has discovered his passion for the software development and IT field, specifically in SaaS and consulting environments. He has previous experience in software-hardware interfacing through his work on the physiological sensing project. He also has management and leadership experience, having supervised over 20 students for their capstone design projects.

Siddiqui Hakim received the B.Eng. and M.Sc. degrees in electrical engineering from McGill University, Montreal, QC, Canada, in 2018 and 2021, respectively. He is currently a Research Associate with the Plant Group, McGill University, and a Co-Founder of a Montreal-based start-up, Stocate. His research interests include biomedical sensing systems, multi-physics-based simulations, and silicon photonic devices.

Nathan Clairmonte received the B.Eng. degree in electrical engineering from McGill University, Montreal, QC, Canada, in 2020, where he is currently pursuing the M.Sc. degree in electrical engineering. His research interests are centered around wearable sensors, biomedical signal processing, data analysis, and machine learning.

Michel A. Lortie received the degree in mechanical engineering from the University of Ottawa. He worked for over 40 years as a Computer and Systems Designer. His design activities have led to implementations in all segments of a modern industrial economy, including manufacturing, process control, aerospace, pharmaceutical, and healthcare industries. His current research interests include clinical decision support systems and cognitive workload assessment. He is a Professional Engineer registered in Ontario and Québec.

David V. Plant (Fellow, IEEE) received the Ph.D. degree from Brown University, Providence, RI, USA, in 1989. He was a Research Engineer at the University of California at Los Angeles, Los Angeles, CA, USA, from 1989 to 1993, and has been a Professor at McGill University, Montreal, QC, Canada, since 1993, where he holds a James McGill Professorship. He has published more than 400 journals and conference papers and has one licensed patent. He is a Fellow of OSA, Engineering Institute of Canada, and the Canadian Academy of Engineering. He currently holds a Killam Research Fellowship. He has received five teaching awards and numerous other awards, including the IEEE Photonics Society Distinguished Lectureship and the IEEE Microwave Theory and Techniques Society Microwave Prize.